THE JOURNAL OF BIOLOGICAL CHEMISTRY VOL. 281, NO. 9, pp. 5973–5981, March 3, 2006

Structure of Microsomal Cytochrome P450 2B4 Complexed with the Antifungal Drug Bifonazole

INSIGHT INTO P450 CONFORMATIONAL PLASTICITY AND MEMBRANE INTERACTION[*] [S]

Received for publication, October 21, 2005, and in revised form, December 12, 2005 Published, JBC Papers in Press, December 21, 2005, DOI 10.1074/jbc.M511464200

Yonghong Zhao[‡1], **Mark A. White**[§2], **B. K. Muralidhara**[‡], **Ling Sun**[‡], **James R. Halpert**[‡], **and C. David Stout**[¶]

From the [‡]*Department of Pharmacology and Toxicology and the* [§]*Sealy Center for Structural Biology, University of Texas Medical Branch, Galveston, Texas 77555 and the* [¶]*Department of Molecular Biology, The Scripps Research Institute, La Jolla, California 92037*

To better understand ligand-induced structural transitions in cytochrome P450 2B4, protein-ligand interactions were investigated using a bulky inhibitor. Bifonazole, a broad spectrum antifungal agent, inhibits monooxygenase activity and induces a type II binding spectrum in 2B4dH(H226Y), a modified enzyme previously crystallized in the presence of 4-(4-chlorophenyl)imidazole (CPI). Isothermal titration calorimetry and tryptophan fluorescence quenching indicate no significant burial of protein apolar surface nor altered accessibility of Trp-121 upon bifonazole binding, in contrast to recent results with CPI. A 2.3 Å crystal structure of 2B4-bifonazole reveals a novel open conformation with ligand bound in the active site, which is significantly different from either the U-shaped cleft of ligand-free 2B4 or the small active site pocket of 2B4-CPI. The O-shaped active site cleft of 2B4-bifonazole is widely open in the middle but narrow at the top. A bifonazole molecule occupies the bottom of the active site cleft, where helix I is bent ~15° to accommodate the bulky ligand. The structure also defines unanticipated interactions between helix C residues and bifonazole, suggesting an important role of helix C in azole recognition by mammalian P450s. Comparison of the ligand-free 2B4 structure, the 2B4-CPI structure, and the 2B4-bifonazole structure identifies structurally plastic regions that undergo correlated conformational changes in response to ligand binding. The most plastic regions are putative membrane-binding motifs involved in substrate access or substrate binding. The results allow us to model the membrane-associated state of P450 and provide insight into how lipophilic substrates access the buried active site.

Cytochromes P450[3] of the 1, 2, and 3 families play a central role in drug metabolism and detoxification (1). Unlike most classical enzymes with their strict substrate selectivity, these microsomal P450s can each bind and metabolize a number of substrates that are different in size, shape, and stereochemistry. A challenging problem is to understand how microsomal P450s accommodate different substrates and oxidize each in a regiospecific and stereo-specific manner. At the tertiary structural level, P450s exhibit a similar overall fold with a well conserved heme-binding core (2). However, recent results demonstrate that microsomal P450s exhibit striking conformational diversity and plasticity (3–5). Not only do different P450s exhibit different conformations, but an individual P450 can adopt multiple conformations in response to various ligands, making it difficult to model protein-ligand interactions even when one atomic structure of a P450 is known. Therefore, a good sampling of P450 "conformational space" is a prerequisite for understanding P450-ligand interactions and for performing modeling studies with high predictive power.

P450s from the 2B subfamily are inducible by barbiturates and have been the object of numerous biochemical and biophysical investigations for several decades. P450 2B4, in particular, was the first microsomal P450 to be purified and is one of the best characterized xenobiotic metabolizing P450s (6). Recent structural investigations using an N-terminal modified form of P450 2B4 (2B4dH) have revealed that the enzyme can adopt strikingly different conformations (4, 5), making it one of the best sources for study of P450 conformational plasticity. In addition, a wealth of site-directed mutagenesis data on 2B4 and other 2B enzymes are available to correlate structural features with functional properties (7). When P450 2B4dH was crystallized without ligand, a tight dimer was formed by two symmetrical molecules that each adopted a widely open conformation (4). A large cleft is formed by helices F through G on one side and the B′/C loop and helix C on the other side (Fig. 1*A*). The cleft is ~15 Å wide and is filled by helices F′ and G′ of the symmetry-related molecule, whose His-226 forms an intermolecular coordinate bond to the heme iron of the other monomer. In order to investigate the structure of 2B4 with a ligand bound, the H226Y mutant was created to minimize dimer formation (5). When 2B4dH(H226Y) was crystallized with the inhibitor 4-(4-chlorophenyl)imidazole (CPI), a closed conformation was observed (Fig. 1*B*), which resembles those of P450s 2C5 (8–10), 2C8 (11), 2C9 (12, 13), and 3A4 (14, 15). The B′/C loop and the N terminus of helix I move toward the active site, making contact with CPI. Helices F through G move toward the B′ helix and cap the top of the active site. The ligand-free 2B4 structure and the 2B4-CPI structure have significantly advanced our knowledge of the structure and function of microsomal P450s. However, CPI (178.6 Da) is the smallest ligand that has been structurally characterized in a mammalian P450 active site, and the compound is highly constrained by the enzyme on all sides. Accordingly, it is impossible to accommodate any larger

* This work was supported in part by National Institutes of Health Grants ES03619 (to J. R. H.) and GM61545 (to C. D. S.) and NIEHS Center Grant ES06676 (to J. R. H.). The costs of publication of this article were defrayed in part by the payment of page charges. This article must therefore be hereby marked "*advertisement*" in accordance with 18 U.S.C. Section 1734 solely to indicate this fact.

The atomic coordinates and structure factors (code 2BDM) have been deposited in the Protein Data Bank, Research Collaboratory for Structural Bioinformatics, Rutgers University, New Brunswick, NJ (http://www.rcsb.org/).

[S] The on-line version of this article (available at http://www.jbc.org) contains Figs. S1 and S2.

[1] To whom correspondence should be addressed. Tel.: 409-772-9670; Fax: 409-772-9642; E-mail: yozhao@utmb.edu.

[2] Supported by Sealy and Smith Foundation for Medical Research.

[3] The abbreviations used are: P450, cytochrome P450; P450 2B4dH, P450 2B4 modified by truncation and modification of the N-terminal transmembrane motif and addition of a C-terminal His tag; CPI, 4-(4-chlorophenyl)imidazole; ITC, isothermal titration calorimetric; Cymal-5, cyclohexyl-pentyl-β-D-maltoside; 7-EFC, 7-ethoxy-4-trifluoromethylcoumarin; MES, morpholinoethanesulfonic acid; PR, plastic regions; SRS, substrate recognition site.

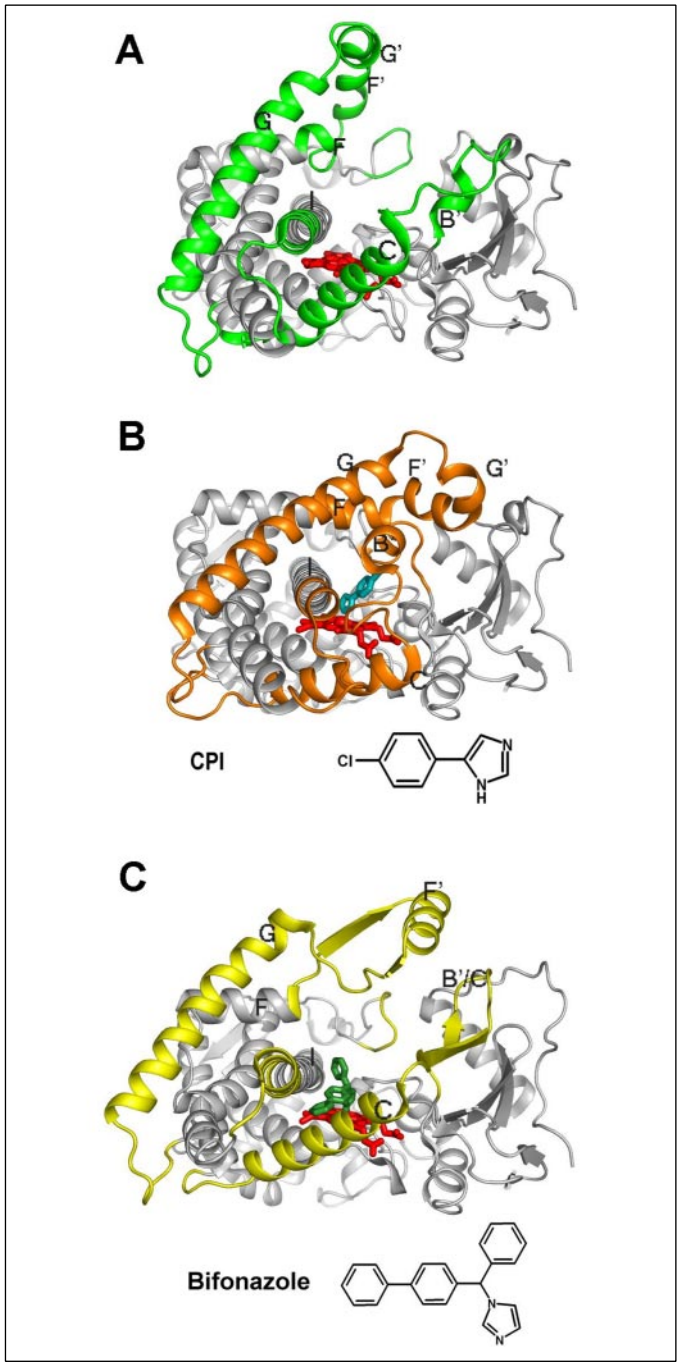

FIGURE 1. *A*, structure of ligand-free 2B4. *B*, structure of 2B4-CPI. The chemical formula of CPI is shown below the protein structure. *C*, structure of 2B4-bifonazole. The chemical formula of bifonazole is shown below the protein structure. The three structures are shown in the same orientation by aligning the most conserved tertiary structure (residues 61–98 and 306–465). Four regions around the active site (residues 100–140, 203–262, 276–290, and 474–479) are colored *green* in *A*, *orange* in *B*, and *yellow* in *C*, respectively, with the major helices labeled. Other parts of the protein are colored *gray* in all three structures. Heme, CPI, and bifonazole are shown as *red*, *cyan*, and *forest green sticks*, respectively. Images were generated using PyMol (www.pymol.org) unless otherwise credited.

ligands in the 2B4-CPI active site without substantial reorganization. We reasoned that structures of 2B4 bound with bulkier ligands should reveal new insights into the conformational changes required to reconstruct the active site.

Azole-containing compounds are well established drugs for the treatment of fungal infections in both humans and animals (16). These drugs inhibit cytochrome P450 14α-demethylase (CYP51), an essential enzyme that converts lanosterol to ergosterol in fungi (17). Many azole compounds also block host P450s, causing toxic side effects. Bifonazole (1-[phenyl-(4-phenylphenyl)-methyl]imidazole) (Fig. 1*C*) is one such azole drug used in the treatment of fungal skin infections. Initial spectral titration experiments indicated that bifonazole (310.4 Da) binds tightly to 2B4dH(H226Y), suggesting the possibility of an intermediate conformation between the open ligand-free structure and the closed 2B4-CPI structure.

In this study, isothermal titration calorimetry (ITC) (18) and tryptophan fluorescence-quenching experiments were used to investigate the interactions of 2B4dH(H226Y) with bifonazole in solution. The results suggested a very different conformation from 2B4-CPI. Crystallographic studies of 2B4-bifonazole revealed a structure (Fig. 1*C*) that is significantly different from either ligand-free 2B4 or 2B4-CPI. The different conformations of 2B4-CPI and 2B4-bifonazole indicate that helix C and the N-terminal half of helix I are central to enzyme plasticity. Based on analysis of the three 2B4 structures, a model for the membrane-associated state of 2B4 is proposed. The model is consistent with other biochemical and structural information and suggests how mammalian P450s, including P450 3A4, evolved as membrane-associated proteins to gain the conformational plasticity required to act on diverse substrates and to provide access to lipophilic substrates that may reside in the bilayer.

EXPERIMENTAL PROCEDURES

Protein Expression and Purification—Cytochrome P450 2B4dH(H226Y) was expressed and purified as described previously (5). Briefly, *Escherichia coli* transformed with the vector pKK2B4dH(H226Y) was grown at 37 °C with shaking until the A_{600} reached 1.0. Protein expression was induced by the addition of isopropyl 1-thio-β-D-galactopyranoside to Terrific broth. After an induction period of 48–72 h, the cells were harvested and lysed. P450 2B4dH(H226Y) was extracted from membranes by adding the detergent Cymal-5 (Anatrace, Maumee, OH) in high salt buffer. After ultracentrifugation, the supernatant was first purified using metal-affinity chromatography. The fractions containing P450 2B4dH(H226Y) were pooled together and then further purified by ion-exchange chromatography. The final buffer contained 500 mM NaCl, 8% glycerol, 1 mM EDTA, 1 mM dithiothreitol, and 10 mM potassium phosphate, pH 7.4. For crystallization, bifonazole (Sigma) was added to the purified protein in 10-fold excess, and the complex was concentrated by using an Ultra-15 centrifugal device (Millipore, Billerica, MA). For solution experiments, 2B4dH(H226Y) was dialyzed against 50 mM citrate-phosphate, pH 4.5, containing 1 mM tris(2-carboxyethyl)phosphine, 1 mM EDTA, 500 mM NaCl, and 1 mM Cymal-5, and a stock of bifonazole was prepared using the same buffer.

Enzymatic Assays and Solution Studies—*O*-Deethylation of 7-ethoxy-4-trifluoromethylcoumarin (7-EFC) was assayed as described previously (19) with 10 pmol of P450, 40 pmol of NADPH-cytochrome P450 reductase, 20 pmol of cytochrome b_5, and 200 μM 7-EFC in the presence of 0–10 μM bifonazole. The 7-EFC *O*-deethylation activities were plotted in relation to the bifonazole concentrations in SigmaPlot (Systat Software, Inc., Point Richmond, CA). Nonlinear regression analysis was performed to fit the data using a four-parameter logistic function to derive the inhibitory concentration 50% (IC_{50}) value.

Bifonazole was titrated into ~1 μM P450, and difference spectra were recorded on a Shimadzu UV-2600 spectrophotometer at room temperature. The differences between the 433 nm maximum and 411 nm minimum were plotted against the bifonazole concentrations. Nonlinear

regression analysis was performed in KaleidaGraph (Synergy Software, Reading, PA), and the spectral dissociation constant (K_S) was obtained by fitting the data to the equation for "tight binding": $2\Delta A = \Delta A_{max}((K_D + [I_0] + [E_0]) - ((K_D + [I_0] + [E_0])^2 - 4[E_0][I_0])^{1/2})$, where ΔA and ΔA_{max} are differential absorbances at particular and saturating inhibitor concentrations, respectively.

ITC experiments were performed on a VP-ITC calorimeter interfaced with a computer for data acquisition and analysis. Protein concentration was 60 μM, and its monomeric state was confirmed by analytical ultracentrifugation experiments. P450 2B4dH(H226Y) and bifonazole (1 mM stock) were quickly preincubated to 25 °C and loaded into the calorimetric cell and titration syringe, respectively. A typical titration schedule included 30–35 injections of 5 μl of bifonazole spaced at 3-min intervals. The titration cell was continuously stirred at 305 rpm. Reference titrations were carried out by titrating bifonazole into buffer alone in the calorimetric cell with the identical injection schedule, and the heat of dilution was subtracted from the bifonazole-protein titration data. The resulting binding isotherms were fit to a one-set binding site model by Marquardt nonlinear least square analysis to obtain binding stoichiometry (N), association constant (K_a), and thermodynamic parameters of interaction using Origin 7.0 software (Microcal Inc., Northampton, MA).

In acrylamide-quenching experiments, 5 μM 2B4dH(H226Y) was incubated with bifonazole at 25 °C for 1 h at a molar ratio of 1:2 prior to measuring the tryptophan fluorescence on a Fluorolog-3 spectrofluorometer (Jobin-Yvon, Edison, NJ). The tryptophan was excited at 295 nm and emission measured between 310 and 400 nm. Collision quenching was described by the Stern-Volmer equation as follows: $F_0/F = 1 + k_q \tau_0 [Q] = 1 + K_{SV}[Q]$, where F_0 and F are fluorescence intensities in the absence and presence of acrylamide; k_q is the bimolecular quenching constant; τ_0 is the lifetime of the fluorophore in the absence of quencher; $[Q]$ is the concentration of acrylamide, and K_{SV} is the Stern-Volmer constant.

Structure Determination and Analysis—The protein sample was prepared as a 31 mg/ml stock in buffer containing 500 mM NaCl, 8% glycerol, 1 mM EDTA, 1 mM dithiothreitol, 1 mM bifonazole, 4.8 mM Cymal-5, and 10 mM potassium phosphate, pH 7.4. The 2B4-bifonazole complex was crystallized from vapor diffusion hanging drops in which 2 μl of protein sample was mixed with 2 μl of reservoir buffer containing 0.1 M NaH_2PO_4, 0.1 M KH_2PO_4, 1.9–2.2 M NaCl, and 0.1 M MES, pH 6.25. The drops were equilibrated against the reservoir buffer for 3–4 weeks at 18 °C. When the crystals were about 0.15 × 0.15 × 0.2 mm, the crystallization drop was transferred to another well and dehydrated by equilibrating for 2–3 days against 0.1 M NaH_2PO_4, 0.1 M KH_2PO_4, 3.5 M NaCl, and 0.1 M MES, pH 6.5, at 18 °C. Crystals were briefly soaked in the mother liquor supplemented with 15% glycerol and 15% ethylene glycol, followed by flash freezing in liquid N_2.

Initially, 360 frames (0.25°/frame) were collected on a single crystal held at 100 K to a resolution of 3.4 Å using a M06XHF rotating anode x-ray generator and a DIP2030H Imaging Plate detector (MacScience). The data were processed using DENZO and SCALEPACK (20). The resolution was extended to 2.3 Å on a dehydrated crystal at beam line 9-1 of the Stanford Synchrotron Radiation Laboratory (Stanford, CA) using a Quantum-315 CCD detector (Area Detector Systems Corp.). One hundred eighty frames (0.5°/frame) collected at 100 K were processed using MOSFLM (21) and SCALA (22). Data collection and processing statistics are shown in Table 1.

Preliminary crystallographic analysis indicated that 2B4-bifonazole crystals belong to space group $P6_122$ or $P6_522$. A molecular replacement search model was constructed by making an ensemble from both the ligand-free 2B4 structure (4) and the 2B4-CPI structure (5) using the PHASER program (23, 24). The top solution of the rotation function had a Z-score of 5.10. Translational search was performed for both $P6_122$ and $P6_522$ space groups. The top solution had a Z-score of 21.91 and was in space group $P6_122$. The molecular replacement solution from PHASER was used for rigid body refinement in CNS (25), which resulted in an R-factor of 36.7%. An electron density map was calculated after solvent flattening using RESOLVE (26). Most of the protein backbone could be traced, and the electron density of the inhibitor in the active site was visible. However, multiple regions including helices B′ through C and helices F through I did not fit the density. They were removed from the starting model and rebuilt manually into the map using the Xfit module of XtalView (27). Cycles of model building and minimization in CNS (28) were performed to refine the coordinates. Bifonazole, Cymal-5, and water molecules were added into the model after most protein residues were well defined. The structural topology and parameters of bifonazole and Cymal-5 were generated using the PRODRG web server (29). The final model contains protein residues 28–492, 3 molecules of bifonazole, 4 molecules of Cymal-5, and 131 water molecules. Refinement was carried out using CNS (28) with the PMB (5) suite of structure refinement utilities (www.x-ray.utmb.edu/PMB.html). Refinement and model statistics are shown in Table 1. Structure evaluation with PROCHECK (30) indicated that the final model has good stereochemistry with no residues in disallowed regions of the Ramachandran plot (Table 1). The average B-factor of three bifonazole molecules is comparable with the average B-factor of protein residues. Two Cymal-5 molecules near the active site are well ordered. The maltose head groups of the other two Cymal-5 molecules extend out of the protein surface and are disordered, giving rise to the high

TABLE 1
Data collection and refinement statistics

Crystal	
Construct	2B4dH(H226Y)
Complex	Bifonazole
Space group	$P6_122$
Unit cell (Å)	
$a = b$	203.21
c	103.45
Data collection	
SSRL beamline	9-1
Wavelength (Å)	0.98
Resolution range[a] (Å)	28.5–2.3 (2.36–2.3)
Total observations[a]	556,804 (34,629)
Unique reflections[a]	52,060 (4,067)
Completeness[a]	99.9 (99.9)
Redundancy[a]	10.1 (8.5)
$I/\sigma(I)$[a]	7.7 (1.6)
R_{sym}[a,b]	0.082 (0.467)
Refinement	
Resolution range (Å)	20–2.3
R-factor (%)	19.6
R_{free} (%)	21.5
Root mean square deviations	
Bond lengths (Å)	0.006
Bond angles (°)	1.297
Average B-factors (Å^2)	**63.8**
Protein	61.7
Heme	41.4
Bifonazole	67.4
Cymal-5	111.6
Water	55.4
Ramachandran (%)	
Most favored	89.5
Additional allowed	9.5
Generously allowed	1.0
Disallowed	0

[a] Values for the outer resolution shell of data are given in parentheses.
[b] $R_{sym} = \Sigma|I_i - I_m|/\Sigma I_i$, where I_i is the intensity of the measured reflection and I_m is the mean intensity of all symmetrically related reflections.

average *B*-factor of Cymal-5. The atomic coordinates have been deposited in the Protein Data Bank.

The distances between Cα atoms and the heme iron were calculated for the ligand-free 2B4 structure (4), the 2B4-CPI structure (5), and the 2B4-bifonazole structure, respectively. For each residue, a standard deviation was calculated from its Fe-Cα distances in three 2B4 structures using the equation S.D. = $(\Sigma(d - \text{avg}(d))^2/(n-1))^{1/2}$, where d is the Fe-Cα distance in each structure, avg(d) is their average, and n equals 3. Structurally plastic regions (PR) were identified when most residues (>90%) in a sequential segment had S.D. values greater than 1 Å (an arbitrary cutoff). Note that this one-dimensional calculation underestimates the conformational change when a residue moves without changing its Fe-Cα distance. Overall, the analysis identified the plastic regions efficiently, because conformational changes are clustered. This analysis does not require superposition of the structures; thus no bias is introduced because of the choices of superposition.

RESULTS

Bifonazole Binds to 2B4dH(H226Y) and Inhibits Its Monooxygenase Activity—Binding of bifonazole to 2B4dH(H226Y) induced type II difference spectra with a peak at 433 nm and a trough at 411 nm (Fig. S1*A*), characteristic of nitrogen coordination to the heme iron. Titration of the enzyme with increased bifonazole concentrations defines a K_S of 0.13 μM (Fig. S1*B*). Binding of bifonazole to 2B4dH(H226Y) inhibits its 7-EFC *O*-deethylation activity with an IC_{50} of 0.9 μM (Fig. S1*C*).

With care to maintain 2B4dH(H226Y) in a monomeric state, ITC has been successfully employed in our laboratory to characterize the binding thermodynamics of imidazole inhibitors with the enzyme.[4] In the case of bifonazole, the thermogram exhibits a monotonic decrease in the exothermic heat of binding with successive injections of bifonazole until saturation is reached (supplemental Fig. S1*D*). The resulting binding isotherm was fit to the single-class of binding-site model (supplemental Fig. S1*E*), yielding a binding site (N) of 0.95 ± 0.02 and an association constant (K_a) of (3.2 ± 0.1) × 10^5 M. The enthalpy change (ΔH) and entropy change (ΔS) obtained from the fit were −17.6 kcal mol^{-1} and −33.8 cal mol^{-1} K^{-1}, respectively. The large negative value of ΔH indicates that bifonazole binding is enthalpically driven and largely hydrophobic. The large negative value of ΔS implies that the binding is entropically unfavorable, and no significant burial of protein apolar surface is induced upon bifonazole binding. In contrast, CPI binding is entropically favorable and induces burial of a large protein apolar surface.[4]

Acrylamide quenching of tryptophan fluorescence indicated that CPI binding to 2B4dH(H226Y) significantly decreases the solvent accessibility of the sole tryptophan (Trp-121),[4] probably because of the large scale relocation of helix C bearing this residue (4, 5). In acrylamide-quenching experiments, the Stern-Volmer constants were 3.3 M^{-1} for ligand-free 2B4 and 3.4 M^{-1} for 2B4-bifonazole, respectively. These results show that, unlike CPI, bifonazole binding does not change the solvent accessibility of Trp-121 significantly. Thus, both the ITC and fluorescence studies suggested a conformation of 2B4-bifonazole distinct from that of 2B4-CPI.

The Overall Structure of the 2B4-Bifonazole Complex—The structure of 2B4-bifonazole was determined from data collected on a single crystal diffracting to 2.3 Å. The complex crystallized in the $P6_122$ space group with one molecule per asymmetric unit. The monomer exhibits the typical P450 fold (Fig. 2*A*). Two monomers related by a crystallographic 2-fold axis form a dimer with the regions between helices F and G of one molecule inserting into the active site of the other molecule and vice versa. Residues 101–116 between helices B and C and residues 204–227 between helices F and G form most of the interaction on the dimer interface (Fig. 2*B*). An intermolecular anti-parallel β-sheet β′6 is formed by residues 206–210 (strand $\beta'_{6\text{-}1}$) of both monomers. Another intermolecular β-sheet β′7 is formed by residues 222–224 ($\beta'_{7\text{-}1}$), 101–103 ($\beta'_{7\text{-}2}$), and 112–116 ($\beta'_{7\text{-}3}$) of both monomers. Helix F′, extending ~35 Å from the heme on strands $\beta'_{6\text{-}1}$ and $\beta'_{7\text{-}1}$, is buried in the active site cleft of the symmetry-related molecule (Fig. 2*B*). All cofactors (bifonazole and Cymal-5), except one Cymal-5, are present at the dimer interface and interact with the symmetry-related molecules.

The 2B4-bifonazole dimer is different from the ligand-free 2B4dH dimer, which involves the coordination of His-226 to the heme iron of the other monomer (4). The protein used in this study has the H226Y mutation, which abolishes the strong His-Fe intermolecular interaction (5). In ITC experiments, the mutated enzyme (60 μM) existed as a monomer in the presence of Cymal-5 and bifonazole, as evidenced by ultracentrifugation experiments. It is likely that the 2B4-bifonazole dimer is formed to sequester hydrophobic surface area at the high protein concentration used in crystallization experiments.

Bifonazole Binding Sites—There are three bifonazole molecules bound to the protein (Fig. 2*A*). One bifonazole is located in the active site, and bifonazole molecules in association with Cymal-5 molecules are found in two hydrophobic pockets away from the active site. These cofactors seem to be beneficial for crystallization, because they are present at the crystallographic dimer interface (Fig. 2*B*). Bifonazole binding to the two distal hydrophobic sites appears to be low affinity, because it was not detected in the ITC experiments. The functional relevance of these two additional binding sites is unclear.

The type II binding spectrum observed in solution presumably derives from the bifonazole molecule in the active site with an imidazole nitrogen coordinated to the heme iron at a bond distance of 2.1 Å (Fig. 3*A*). The imidazole ring of bifonazole makes contact with Thr-302 and Ile-363, which belong to substrate recognition sites (SRS) 4 and 5 (31), respectively. In both 2B4-bifonazole and 2B4-CPI, the imidazole ring is approximately vertical to the plane of the heme. At the same time, the bifonazole imidazole ring is almost parallel to helix I, whereas the CPI imidazole ring is at an ~60° angle with helix I. Like flurbiprofen in P450 2C9 (13), bifonazole binds across the length of helix I and makes contact with seven helix I residues Val-292, Leu-295, Phe-296, Ala-298, Gly-299, Glu-301, and Thr-302 (Fig. 3*A*). The biphenyl rings of bifonazole are located between the heme and helix I, which is bent ~15° to accommodate the ligand. The first phenyl ring stacks on the heme and positions the second phenyl ring toward helix C, making contact with Ser-128 and Met-132. The F′ helix of the symmetry-related molecule packs on top of the active site bifonazole, isolating it from solvent regions. On the opposite side of helix I, bifonazole interacts extensively with the hydrophobic tail of a Cymal-5 molecule and side chains of helix F′ residues Val-216, Phe-217, and Phe-220.

Ten residues (Ile-101, Ile-114, Phe-115, Phe-297, Ala-298, Glu-301, Thr-302, Ile-363, Val-367, and Val-477) were identified as active site residues in the 2B4-CPI structure (5). Because the active site is reconstructed dramatically, only four of them (Ala-298, Glu-301, Thr-302, and Ile-363) also make contact with bifonazole. Although Val-367 maintains its position, it is about 6 Å away from bifonazole because of the different orientation relative to CPI. Phe-297 is moved out of the active site because of bending of helix I. Ile-101, Ile-114, Phe-115, and Val-477 have moved more than 10 Å away from the ligand, because the

[4] Muralidhara, B. K., Negi, S., Chin, C. C., Braun, W., and Halpert, J. R. (January 26, 2006) *J. Biol. Chem.* 10.1074/jbcM09696200.

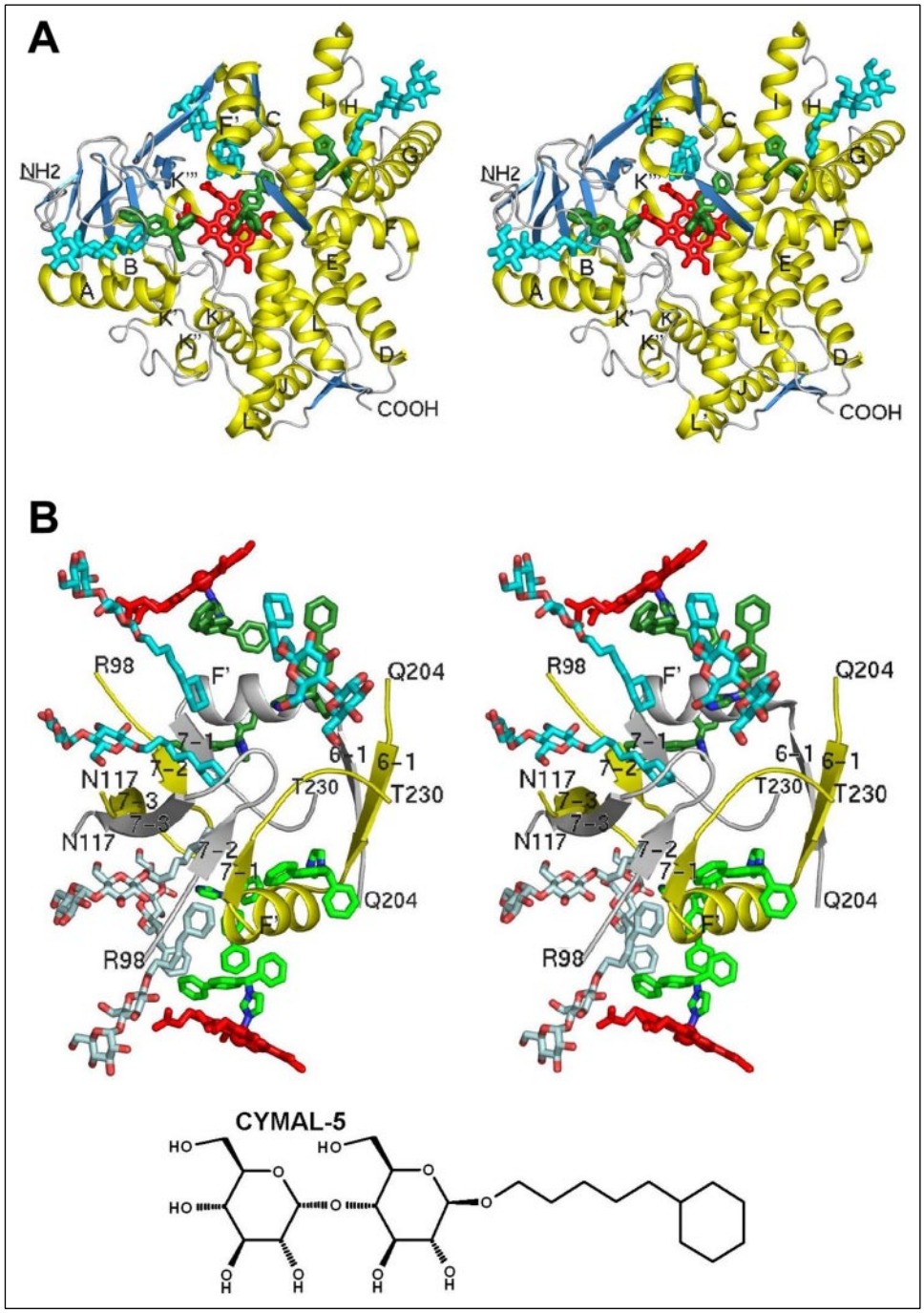

FIGURE 2. *A,* divergent stereo view of the 2B4-bifonazole monomer. Helices and strands are colored *yellow* and *blue,* respectively. The termini and major helices are labeled. Heme, bifonazole, and Cymal-5 molecules are shown as *red, forest green,* and *cyan sticks*, respectively. *B,* the dimer interface of 2B4-bifonazole is stabilized by interdigitating β-strands, and extra copies of detergent and substrate that associate with exposed hydrophobic regions. For clarity, only residues 98–117 and 204–230 are shown. Molecules A and B are colored *yellow* and *gray*, respectively. Heme is shown as *red sticks*. Bifonazole and Cymal-5 of molecule A are shown as *forest green* and *cyan sticks*, respectively. Bifonazole and Cymal-5 of molecule B are shown as *green* and *pale cyan sticks*, respectively. Helix F′ and β-strands 6-1, 7-1, 7-2, and 7-3 are labeled. The chemical formula of Cymal-5 is shown.

B′/C loop and the β4 hairpin adopt different conformations in the 2B4-bifonazole structure.

Heme-binding Site—Although the spatial orientation and conformation of the heme are well conserved, coordination of the heme D ring propionate can be quite different in the different 2B4 structures (Fig. 3*B*). Residues Ser-430 and His-369, which coordinate the heme A ring propionate, align well in both 2B4-CPI and 2B4-bifonazole. In the 2B4-bifonazole structure, Arg-98 switches position and no longer makes contact with the heme A and D ring propionates. Instead, a water molecule is located between the heme A and D ring propionates and forms hydrogen bonds with them. In the 2B4-bifonazole structure, the ligand pushes the C helix away from the heme. As a result, Trp-121 and Arg-125, which are involved in the heme D ring propionate coordination in the 2B4-CPI structure, no longer make contact with the heme. A Cymal-5 molecule inserts between the heme and helix C. The maltose head of the Cymal-5 forms two hydrogen bonds with the heme D ring propionate, stabilizing its conformation (Fig. 3*B*).

The different locations of helix C observed in the 2B4-CPI structure and the 2B4-bifonazole structure are consistent with the results of fluorescence-quenching experiments, based on the corresponding positions of Trp-121. Although helix C is located differently, the C/D loop adopts a similar "looping out" conformation in the 2B4-CPI structure and the 2B4-bifonazole structure (Fig. 3*A*). In contrast, the C/D loop in the ligand-free 2B4 structure is short and directly connects helices C and D. It appears that both bifonazole and CPI induce similar conformational changes of the C/D loop, which may play a role in coupling

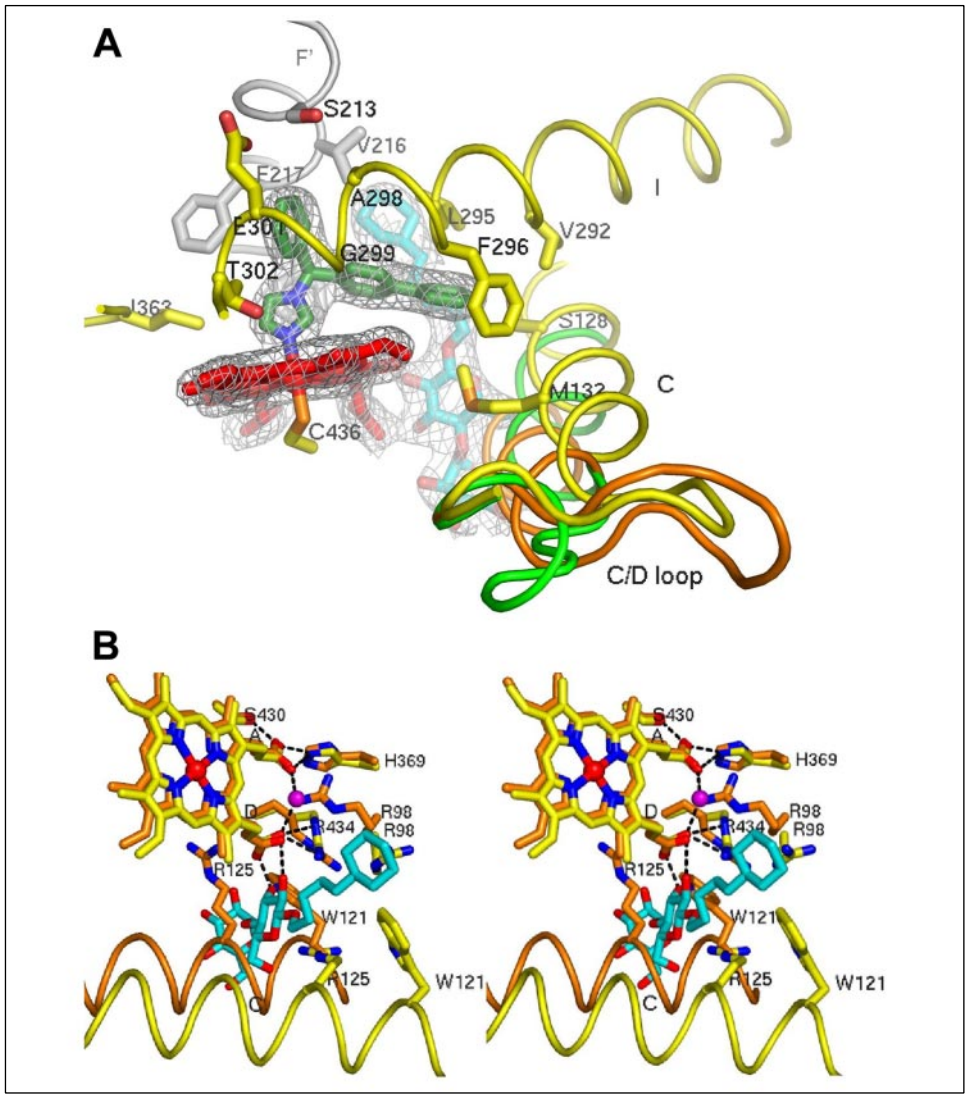

FIGURE 3. *A,* bifonazole in the active site of 2B4. Side chains of residues within a generous 5 Å contact distance from bifonazole are shown as *sticks* and colored by elements (*yellow* indicates carbon, *red* indicates oxygen, and *blue* indicates nitrogen). The carbon atoms of bifonazole and Cymal-5 are colored *forest green* and *cyan*, respectively. Heme is shown as *red sticks*. The carbon atoms of the symmetry-related molecule in the dimer are colored *gray*. The σ_A-weighted $2|F_o| - |F_c|$ omit map is contoured at 1σ and rendered as *gray mesh* for heme, bifonazole, and Cymal-5. Helices I and C and the C/D loop are shown as *ribbons* and are labeled. Helix C and the C/D loop of ligand-free 2B4 (*green*) and 2B4-CPI (*orange*) are also shown. *B*, divergent stereo view of heme coordination. Heme and side chains of residues involved in coordination of heme propionates are shown as *sticks* and colored by elements (*yellow* indicates carbon, *red* indicates oxygen, and *blue* indicates nitrogen). These residues in the 2B4-CPI structure are also shown, and their carbon atoms are colored *orange*. Carbon atoms of Cymal-5 are colored *cyan*. A water molecule is shown as a *magenta sphere*. Hydrogen bonds are depicted as *black dashes*. Helix C is shown as *ribbon*. For all superpositions, the structures were aligned by the most conserved tertiary structure (residues 61–98 and 306–465) unless otherwise stated.

ligand-induced conformational changes with electron delivery from cytochrome P450 reductase to P450 in the case of substrates (5).

Conformational Plasticity of Cytochrome P450 2B4—The S.D. values of Fe-Cα distances in the three 2B4 structures identified structurally conserved and structurally PR (supplemental Fig. S2). There are large structural variations (S.D. >1 Å, an arbitrary cutoff) in five plastic regions as follows: PR1 (residues 39–57), PR2 (residues 101–140), PR3 (residues 177–188), PR4 (residues 203–298), and PR5 (residues 474–480). The N-terminal proline-rich region, the C terminus of helix A, helix B, the C-terminal half of helix I, helices J through L, and all intramolecular β-sheets exhibit the least structural variations (S.D. < 0.3 Å) in the three 2B4 structures. These regions form the protein core, including most of the secondary structural elements that coordinate the heme. In addition, many of these elements are located on the proximal side of the protein, which is implicated in binding of electron transfer partners cytochrome P450 reductase and cytochrome b_5 (32). Overall, these structurally conserved regions of 2B4 account for about 2/3 of the protein and are likely responsible for maintaining the overall P450 fold, coordination of heme, and binding of electron transfer partners.

PR1 comprises residues 39–57, which form a loop preceding helix A and the N-terminal half of helix A (Fig. 4*A*). In the 2B4-bifonazole structure, the helix A backbone has moved away from the protein core by ~4 Å at its N terminus because of the tilt of helix A around its C terminus. The conformational change of PR1 is correlated with that of PR5. In the 2B4-CPI structure, PR5 forms the β4 hairpin, which is located near the C terminus of helix A (Fig. 4*A*). Val-477 of the highly conserved GVG motif is at the tip of the β4 hairpin, making contact with CPI. The β4 hairpin unfolds and becomes a loop in the 2B4-bifonazole structure. As a result, Val-477 moves ~3 Å away from the active site and no longer makes contact with the ligand. The loop conformation of PR5 and the tilt of helix A are partially stabilized by a hydrogen-bond network among the backbones of Ser-475, Gly-476, and Gly-478 and the side chains of Arg-48 and Asn-479, providing a mechanism to correlate the conformational change of PR1 with that of PR5.

PR2 includes helix B′, the B′/C loop, helix C, and the C/D loop (Fig. 4*B*). The B′/C loop makes limited intramolecular contacts and is one of the most conformationally dynamic components of 2B4. In the 2B4-CPI structure, the B′ helix and the B′/C loop are close to the active site, and residues Ile-114 and Phe-115 make contact with the ligand. In the 2B4-bifonazole structure, the B′ helix unravels and refolds into an extended anti-parallel β loop ($\beta'_{7\text{-}2} \uparrow \beta'_{7\text{-}3} \downarrow$). As a result, Ile-114 and Phe-115 are positioned far away from the active site. A large scale shift of helix C is observed when the protein adopts different conformations (Fig. 3, *A* and *B*).

The C-terminal half of helix E is the major secondary structural element of PR3 and exhibits significant structural variations because of

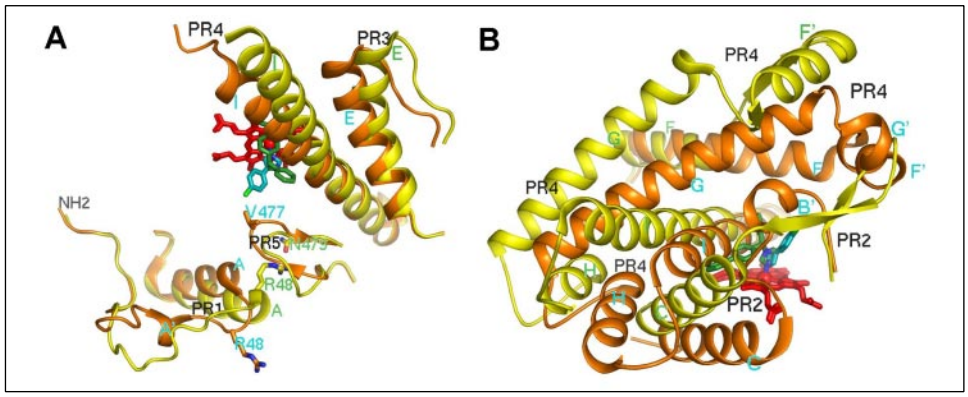

FIGURE 4. **PR of 2B4 exhibit correlated conformational change upon ligand binding.** *A*, superposition of PR1, PR3, PR5, and helix I of 2B4-bifonazole (*yellow*) and 2B4-CPI (*orange*). *B*, superposition of PR2 and PR4 of 2B4-bifonazole (*yellow*) and 2B4-CPI (*orange*). In the bifonazole complex, opening of the structure is associated with refolding and shifting of the B′, F, F′, and G′ regions and repositioning of the C, G, H, and I helices. Major helices are labeled. The positions of PR are indicated. In both panels, heme atoms, bifonazole carbon atoms, and CPI carbon atoms are shown as *red, forest green,* and *cyan sticks*, respectively. Selected side chains of Arg-48, Val-477, and Asn-479 in *A* are shown as *sticks* and colored by elements as follows: *yellow* indicates carbon (*orange* indicates carbon atoms of 2B4-CPI).

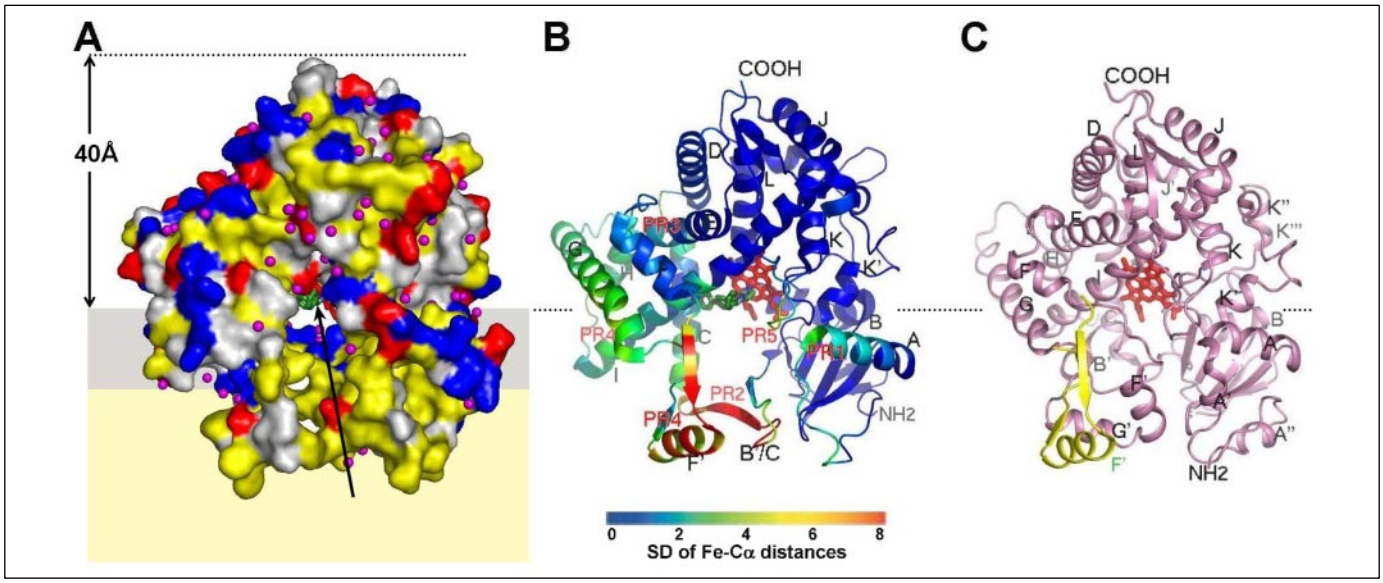

FIGURE 5. **A model for how P450 2B4 may interact with phospholipid bilayers.** The model indicates how the most conformationally dynamic components of the protein fold could be associated with membrane binding, and how this would facilitate substrate binding. *A*, the solvent-accessible surface of the 2B4-bifonazole structure is shown in the putative membrane binding orientation. The surface is colored according to the property of the underlined residues: *yellow* indicates hydrophobic residues (Ala, Gly, Ile, Leu, Met, Pro, Val, Phe, Tyr, and Trp); *white* indicates polar residues (His, Asn, Gln, Ser, Thr, and Cys); *red* indicates negatively charged residues (Asp and Glu); and *blue* indicates positively charged residues (Lys and Arg). Ordered water molecules on the protein surface are shown as *magenta spheres*. The *light gray* and *light yellow boxes* represent the polar region and hydrophobic core region of the phospholipid bilayer, respectively. The approximate height of the protein above the membrane is shown. A possible substrate access channel is indicated by an *arrow*. *B*, the 2B4-bifonazole structure is oriented as in *A* with residues colored according to S.D. value of Fe-Cα distances, ranging from *blue* minimum to *red* maximum (see "Materials and Methods"). Heme and bifonazole are shown as *red* and *forest green sticks*, respectively. Major helices are labeled. The positions of termini and PR are indicated. *C*, the structure of P450 3A4 (Protein Data Bank code 1TQN) is shown in the same orientation with respect to the membrane based on superposition. The termini and major helices are labeled. Heme is shown as *red sticks*. In this orientation, helix G′ of 3A4 would be positioned in the hydrophobic region of phospholipid bilayer, as deeply as helix F′ of 2B4 (*yellow*).

bending of this helix (Fig. 4*A*). The bend originates in the middle of helix E and is stabilized by two hydrogen bonds between the side chain of Asn-177 and the backbone of Phe-188 in the 2B4-bifonazole structure.

PR4 is a large plastic region and comprises the C-terminal half of helix F through the N-terminal half of helix I (Fig. 4*B*). In the 2B4-bifonazole structure, a dramatic extrusion of helix F′ is supported by extension of the C terminus of helix F into a β-strand and unraveling of helix G′ into a β-strand. The bending of helix I, which runs underneath the F and G helices, is a common feature in P450s (33). The C-terminal half of helix I is rigid. The bending of helix I originates at its middle and is likely to be influenced by ligand binding. In the ligand-free 2B4 structure, helix I is slightly bent. Upon bifonazole binding, helix I is further bent to ~15° to accommodate the biphenyl rings of bifonazole. In contrast, CPI binding straightens helix I (Fig. 4*B*).

It appears that the shift of helix C together with the bending of helix I are central to the conformational transitions of PR2, PR3, and PR4. Although helices E, H, and G do not interact directly with the ligands, they move along with helix C and the N terminus of helix I to maintain the relative packing.

DISCUSSION

The anti-fungal drug bifonazole binds tightly to P450 2B4dH(H226Y), as evidenced by a type II binding spectrum, ITC experiments, and inhibition studies. The tight binding facilitated the crystallization of a 2B4-bifonazole complex, which revealed a novel ligand-bound but open conformation, in contrast to the open ligand-free and closed CPI-bound structures determined previously (4, 5). The 2B4-bifonazole structure provides new insight into ligand binding and structural plasticity of 2B4.

The 2B4-bifonazole structure identified 10 residues (Ser-128, Met-132, Val-292, Leu-295, Phe-296, Ala-298, Gly-299, Glu-301, Thr-302, and Ile-363) within 5 Å of the active site bifonazole. Ala-298, Glu-301, Thr-302, and Ile-363 are also located within 5 Å of the bound ligand in the 2B4-CPI structure. These four residues belong to SRS-4 and SRS-5

(31). They are positioned immediately above the heme plane, corresponding to Tier 1 of the $P450_{cam}$ active site (34). Because SRS-5 and the C-terminal half of SRS-4 are structurally conserved (supplemental Fig. S2), it is likely that they play a dominant role in determining regiospecificity and stereospecificity of P450s. CPI-contacting residues Phe-115, Phe-297, Val-477, and Ile-101 correspond to Tier 2 and Tier 3 of the $P450_{cam}$ active site. They do not make contact with bifonazole. Probably the ability to reconstruct Tier 2 and Tier 3 enables microsomal P450s to accommodate ligands of different size and shape. The substrate profile of a given P450 can be determined in part by the combined effect of structurally more rigid Tier 1 with structurally more variable Tier 2 and Tier 3 elements. Although not identified as a substrate recognition region of family 2 P450s (31), helix C has been implicated in azole recognition in both fungal and mammalian P450s (35–37). The direct interaction of 2B4 helix C residues (Ser-128 and Met-132) with bifonazole suggests an important role of helix C in azole recognition by mammalian P450s.

The microsomal P450s are integral membrane proteins with a single transmembrane helix. Beside the N-terminal transmembrane helix, other regions of 2B4 that likely interact with the membrane include the loop before helix A, the B′/C loop, and residues between helices F and G (8). When the 2B4-bifonazole structure is depicted in the putative membrane binding orientation (8), the top and middle of the protein surfaces are hydrophilic, and most hydrophobic surfaces are located at the bottom where the protein is less hydrated (Fig. 5*A*). One could view the 2B4-bifonazole structure as representing a snapshot of a membrane-bound 2B4 conformation with helix F′ deeply embedded into the membrane. Several lines of evidence favor the physiological relevance of this conformation. First, the hydrophobic surfaces at the bottom are formed by residues 30–45 before helix A, the $\beta_{1\text{-}1}$-$\beta_{1\text{-}2}$ loop, residues 101–116 before helix C, helix F′, and flanking residues. Many of these residues have been implicated in membrane binding by antibody binding data (38). Second, the B′/C loop and the F/G region have five phenylalanine residues (Phe-108, Phe-212, Phe-217, Phe-220, and Phe-223), which have a strong tendency to penetrate into the hydrophobic core region of the membrane. Third, many basic residues are located above the hydrophobic regions, where the residues may interact favorably with the head groups of phospholipids in the polar regions of the membrane (Fig. 5*A*). Furthermore, the height of 2B4 above the membrane is about 40 Å in this orientation, within the range of 35 ± 9 Å measured by atomic force microscopy (39).

An intriguing question about P450s is how substrates enter and leave the active site, which is deeply buried in the center of the P450 fold (40). In the putative membrane binding orientation, the 2B4-bifonazole structure exhibits a channel that connects the hydrophobic core of the membrane directly to the active site (Fig. 5*A*). The channel is lined by helix F′ and flanking residues (PR4) on one side, and residues 40–46 before helix A (PR1), residues 101–116 of the B′/C loop (PR2), and residues 476–478 (PR5) on the other side. It is possible that membrane-associated 2B4 adopts a similar conformation to allow lipophilic substrates in the bilayer to access the active site through this channel. The channel also opens to the cytosol, providing access for less lipopholic substrates (note the H_2O molecules above the modeled membrane surface, at the tip of the *arrow*, in Fig. 5*A*).

The three available P450 2B4 structures, when considered together, provide insight to the broad substrate specificities of microsomal P450s. The most conformationally dynamic regions of 2B4, the B′/C loop and the F/G region, are presumably embedded in the membrane and form limited intramolecular interactions (Fig. 5, *A* and *B*). In contrast, the cytosolic moiety of the protein forms extensive intramolecular interactions, which maintain the overall P450 fold, as observed in all three 2B4 structures. With limited intramolecular interactions and yet striking conformational plasticity, it is plausible that the conformations of the putative membrane-binding motifs would be largely dependent on the dynamic lipid environment of the bilayer. Consequently, the ability of the enzyme to embed partially into the membrane in this manner would provide not only a means to sequester lipophilic substrates but also would contribute to versatility in recognition of these substrates.

Structurally extruded membrane-binding motifs are a common feature in other monotopic membrane proteins (41), including oxysterol-binding protein-related proteins (42), phosphatidylinositol transfer protein α (43), prostaglandin H_2 synthase (44, 45), squalene cyclase (46), and estrone sulfatase (47). Because the membrane-binding motifs of 2B4 could also form the ligand access channel (Fig. 5*A*), their conformational plasticity would enable the enzyme to encounter, recognize, and deliver diverse substrates to the active site, without disrupting the overall fold of the catalytic domain. This view of P450 2B4 function infers a similar membrane-associated state of other microsomal P450s. For example, an extended conformation of the F/G region was observed in P450 3A4 (14, 15). In this case, helices A″ and G′ are thought to be embedded in the membrane (Fig. 5*C*), consistent with structural superposition (residues 61–98 and 306–465) and the proposed orientation of 2B4 (Fig. 5, *B* and *C*). Compared with soluble bacterial P450s, which have narrower substrate specificities, it appears that microsomal P450s, by evolving as membrane-associated proteins, have acquired conformational plasticity, allowing them to recognize and metabolize multiple substrates.

Acknowledgments—We thank Drs. David Bolen and Stanley Watowich for access to their ITC and fluorescence instruments. We thank Dr. Christopher Chin for analytical ultracentrifugation experiments. We thank Dr. Emily Scott (University of Kansas), Dr. Jason Yano (The Scripps Research Institute), and the staff at the Stanford Synchrotron Radiation Laboratory for assistance with data collection. Stanford Synchrotron Radiation Laboratory is operated by Stanford University on behalf of the United States Department of Energy, Office of Basic Energy Sciences. The Stanford Synchrotron Radiation Laboratory Structural Molecular Biology Program is supported by the Department of Energy, Office of Biological and Environmental Research, and by the National Center for Research Resources, Biomedical Technology Program, and the National Institute of General Medical Sciences, National Institutes of Health. The Sealy Center for Structural Biology is supported by the Sealy and Smith Foundation for Medical Research.

REFERENCES

1. Rendic, S. (2002) *Drug Metab. Rev.* **34,** 83–448
2. Poulos, T. L. (2005) *Drug Metab. Dispos.* **33,** 10–18
3. Johnson, E. F., and Stout, C. D. (2005) *Biochem. Biophys. Res. Commun.* **338,** 331–336
4. Scott, E. E., He, Y. A., Wester, M. R., White, M. A., Chin, C. C., Halpert, J. R., Johnson, E. F., and Stout, C. D. (2003) *Proc. Natl. Acad. Sci. U. S. A.* **100,** 13196–13201
5. Scott, E. E., White, M. A., He, Y. A., Johnson, E. F., Stout, C. D., and Halpert, J. R. (2004) *J. Biol. Chem.* **279,** 27294–27301
6. Coon, M. J., Hoeven, T. A., Kaschnitz, R. M., and Strobel, H. W. (1973) *Ann. N. Y. Acad. Sci.* **212,** 449–457
7. Domanski, T. L., and Halpert, J. R. (2001) *Curr. Drug Metab.* **2,** 117–137
8. Williams, P. A., Cosme, J., Sridhar, V., Johnson, E. F., and McRee, D. E. (2000) *Mol. Cell* **5,** 121–131
9. Wester, M. R., Johnson, E. F., Marques-Soares, C., Dijols, S., Dansette, P. M., Mansuy, D., and Stout, C. D. (2003) *Biochemistry* **42,** 9335–9345
10. Wester, M. R., Johnson, E. F., Marques-Soares, C., Dansette, P. M., Mansuy, D., and Stout, C. D. (2003) *Biochemistry* **42,** 6370–6379
11. Schoch, G. A., Yano, J. K., Wester, M. R., Griffin, K. J., Stout, C. D., and Johnson, E. F. (2004) *J. Biol. Chem.* **279,** 9497–9503
12. Williams, P. A., Cosme, J., Ward, A., Angova, H. C., Vinkovic, D. M., and Jhoti, H. (2003) *Nature* **424,** 464–468
13. Wester, M. R., Yano, J. K., Schoch, G. A., Yang, C., Griffin, K. J., Stout, C. D., and

Johnson, E. F. (2004) *J. Biol. Chem.* **279,** 35630–35637
14. Williams, P. A., Cosme, J., Vinkovic, D. M., Ward, A., Angove, H. C., Day, P. J., Vonrhein, C., Tickle, I. J., and Jhoti, H. (2004) *Science* **305,** 683–686
15. Yano, J. K., Wester, M. R., Schoch, G. A., Griffin, K. J., Stout, C. D., and Johnson, E. F. (2004) *J. Biol. Chem.* **279,** 38091–38094
16. Bossche, H. V., Koymans, L., and Moereels, H. (1995) *Pharmacol. Ther.* **67,** 79–100
17. Waterman, M. R., and Lepesheva, G. I. (2005) *Biochem. Biophys. Res. Commun.* **338,** 418–422
18. Leavitt, S., and Freire, E. (2001) *Curr. Opin. Struct. Biol.* **11,** 560–566
19. Scott, E. E., Spatzenegger, M., and Halpert, J. R. (2001) *Arch. Biochem. Biophys.* **395,** 57–68
20. Otwinowski, Z., and Minor, W. (1997) *Methods Enzymol.* **276,** 307–326
21. Leslie, A. G. W. (1999) *Acta Crystallogr. Sect. D Biol. Crystallogr.* **55,** 1696–1702
22. Bailey, S. (1994) *Acta Crystallogr. Sect. D Biol. Crystallogr.* **50,** 760–763
23. Storoni, L. C., McCoy, A. J., and Read, R. J. (2004) *Acta Crystallogr. Sect. D Biol. Crystallogr.* **60,** 432–438
24. McCoy, A. J., Grosse-Kunstleve, R. W., Storoni, L. C., and Read, R. J. (2005) *Acta Crystallogr. Sect. D Biol. Crystallogr.* **61,** 458–464
25. Terwilliger, T. C. (2003) *Methods Enzymol.* **374,** 22–37
26. Terwilliger, T. C. (2000) *Acta Crystallogr. Sect. D Biol. Crystallogr.* **56,** 965–972
27. McRee, D. E. (1999) *J. Struct. Biol.* **125,** 156–165
28. Brunger, A. T., Adams, P. D., Clore, G. M., DeLano, W. L., Gros, P., Grosse-Kunstleve, R. W., Jiang, J. S., Kuszewski, J., Nilges, M., Pannu, N. S., Read, R. J., Rice, L. M., Simonson, T., and Warren, G. L. (1998) *Acta Crystallogr. Sect. D Biol. Crystallogr.* **54,** 905–921
29. Schuttelkopf, A. W., and van Aalten, D. M. F. (2004) *Acta Crystallogr. Sect. D Biol. Crystallogr.* **60,** 1355–1363
30. Laskowski, R. A., Macarthur, M. W., Moss, D. S., and Thornton, J. M. (1993) *J. Appl. Crystallogr.* **26,** 283–291
31. Gotoh, O. (1992) *J. Biol. Chem.* **267,** 83–90
32. Bridges, A., Gruenke, L., Chang, Y. T., Vakser, I. A., Loew, G., and Waskell, L. (1998) *J. Biol. Chem.* **273,** 17036–17049
33. Li, H., and Poulos, T. L. (2004) *Curr. Top. Med. Chem.* **4,** 1789–1802
34. Mueller, E. J., Loida, P. J., and Sligar, S. G. (1995) in *Cytochrome P450: Structure, Mechanism, and Biochemistry* (Ortiz de Montellano, P. R., ed) pp. 83–124, Plenum Press, New York
35. Tanaka, T., Kamiguchi, N., Okuda, T., and Yamamoto, Y. (2004) *Chem. Pharm. Bull.* **52,** 836–841
36. Tanaka, T., Okuda, T., and Yamamoto, Y. (2004) *Chem. Pharm. Bull.* **52,** 830–835
37. Matsuura, K., Yoshioka, S., Tosha, T., Hori, H., Ishimori, K., Kitagawa, T., Morishima, I., Kagawa, N., and Waterman, M. R. (2005) *J. Biol. Chem.* **280,** 9088–9096
38. Delemoschiarandini, C., Frey, A. B., Sabatini, D. D., and Kreibich, G. (1987) *J. Cell Biol.* **104,** 209–219
39. Bayburt, T. H., and Sligar, S. G. (2002) *Proc. Natl. Acad. Sci. U. S. A.* **99,** 6725–6730
40. Wade, R. C., Winn, P. J., Schlichting, I., and Sudarko, (2004) *J. Inorg. Biochem.* **98,** 1175–1182
41. Bracey, M. H., Cravatt, B. F., and Stevens, R. C. (2004) *FEBS Lett.* **567,** 159–165
42. Im, Y. J., Raychaudhuri, S., Prinz, W. A., and Hurley, J. H. (2005) *Nature* **437,** 154–158
43. van Tiel, C. M., Schouten, A., Snoek, G. T., Gros, P., and Wirtz, K. W. (2002) *FEBS Lett.* **531,** 69–73
44. Garavito, R. M., Malkowski, M. G., and DeWitt, D. L. (2002) *Prostaglandins Other Lipid Mediat.* **68,** 129–152
45. Smith, W. L., DeWitt, D. L., and Garavito, R. M. (2000) *Annu. Rev. Biochem.* **69,** 145–182
46. Wendt, K. U., Poralla, K., and Schulz, G. E. (1997) *Science* **277,** 1811–1815
47. Hernandez-Guzman, F. G., Higashiyama, T., Pangborn, W., Osawa, Y., and Ghosh, D. (2003) *J. Biol. Chem.* **278,** 22989–22997